Macromolecular Research

Article

DOI 10.1007/s13233-020-8133-x

www.springer.com/13233 pISSN 1598-5032 eISSN 2092-7673

Effect of the Conformation Changes of Polyelectrolytes on Organic Thermoelectric Performances

Kyungwho Choi[1]
Jihun Son[2]
Yong Tae Park[3]
Jung Sang Cho[4]
Chungyeon Cho*[,2]

[1] School of Aerospace & Mechanical Engineering, Korea Aerospace University, Goyang-si, Gyeonggi 10540, Korea
[2] Department of Carbon Convergence Engineering, College of Engineering, Wonkwang University, Iksan 54538, Korea
[3] Department of Mechanical Engineering, Myongji University, 116 Myongji-ro, Cheoin-gu, Yongin, Gyeonggi 17058, Korea
[4] Department of Engineering Chemistry, Chungbuk National University, Gaesin-Dong, Seowon-Gu, Cheongju 28644, Korea

Received February 7, 2020 / Revised May 15, 2020 / Accepted June 6, 2020

Abstract: The relationship between the conformation of a polyelectrolyte and the performance of organic thermoelectric multilayers was studied. The conformational change of a weak polyelectrolyte *via* controlling assembling pH gave rise to a different thermoelectric behaviour in thin films. Organic thermoelectric multilayers were fabricated by alternately depositing bilayers (BL) of a positively-charged polyaniline (PANi) and multiwalled carbon nanotubes (MWNT), stabilized in poly(acrylic acid) (PAA), *via* a layer-by-layer assembly technique. The electrical conductivity and Seebeck coefficient of PANi/MWNT-PAA nanocomposites were measured by varying assembly pH of PAA solutions. Altering the deposition pH of PAA resulted in different thermoelectric performances. A 40 BL thin film (~210 nm thick) of PANi/MWNT-PAA assembled at pH 2.5/6.5 exhibited electrical conductivity of 95.2 S/cm and a Seebeck coefficient of 35 μV/K. This translates to a power factor of 11.7 μW/m·K^2, which is 50 times higher than that of the same film with all components deposited at pH 2.5. Enhancement of thermoelectric behaviour in PANi/MWNT-PAA nanocomposites is attributed to a conjugated π-π network, together with a tightly packed nanostructure.

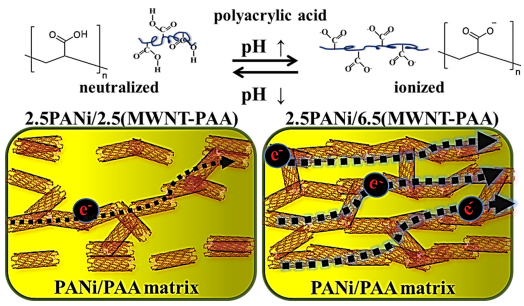

Keywords: layer-by-layer assembly, polyelectrolytes, power factor, electrical conductivity.

1. Introduction

The energy crisis is ongoing and getting worse, as the world demand for energy on the limited natural resources have been rapidly increasing.[1,2] Environmental concerns over traditional energy sources such as fossil fuels stimulate many researchers to find alternative energy sources. To date, various techniques have been developed to harvest energy mechanically, electronically, magnetically, thermally, and biochemically.[3-5] Thermoelectric (TE) materials have been proved to be effective means of converting heat, which is wasted more than half of the energy produced, into useful electricity. The thermoelectric conversion efficiency depends on the dimensionless figure-of-merit (ZT), $ZT = S^2\sigma/\kappa$, where S stands for the Seebeck coefficient (also called the thermopower); σ is electrical conductivity; κ is thermal conductivity; and T is absolute temperature. A power factor (PF = $S^2\cdot\sigma$) is also used to measure the TE performance due to the difficulties in measuring the precise in-plane thermal conductivity for the thin film thickness (< 1 μm).[6] In general, these three physical parameters are strongly correlated with each other (*i.e.*, σ is proportional to κ, while increasing S lowers σ), which imposes limitation on the thermoelectric performance of monolithic materials.[7]

Currently, inorganic materials such as Bi_2Te_3, $CaMnO_3$, Sb_2Te_3, and semiconductor alloys are the most widely used due to their high TE performance (*i.e.*, ZT~2).[8-10] However, these inorganic materials face the challenge for their practical applications because of several drawbacks such as toxicity, high cost, poor mechanical stiffness, material scarcity, and difficulty in processing.[11] Great attention has been paid to organic thermoelectric materials, such as conducting polymers and their composites compounded with carbon nanofillers. In addition to their intrinsically low thermal conductivity, organic materials have multiple advantages including low-cost, easy processing from solutions, flexibility, an readily available resource, and lightweight.[12,13] High thermoelectric performance of inorganic materials typically is achieved at temperatures higher than 500 K, although waste heat dissipated to the environment occurs at low temperature (300 to 500 K).[14] In this regard, organic thermoelectric materials hold much promise for the harvest of low-grade heat.

The thermoelectric properties of organic materials have been dramatically improved by various processing systems such as

Acknowledgment: This research was supported by Wonkwang University in 2020.

***Corresponding Author:** Chungyeon Cho (cncho37@wku.ac.kr)

in-situ polymerization, simple mixing, one-pot fabrication, and polymer-emulsion processing.[15-17] Among these methods, the nanocomposites fabricated by the layer-by-layer (LbL) assembly technique have shown large improvement in power factors due to its precise control over film architecture at a molecular level.[18-20] LbL assembly is a simple method to prepare multifunctional thin films with no restrictions on the size or shape of the substrates used.[21] Sequential exposure of charged substrates into aqueous solutions of complementarily functionalized species yields multilayer films with well-defined structure and thickness.[22] Other than polyelectrolytes, various types of nanomaterials such as carbon nanomaterials, micelles, biomolecules, and nanoparticles are used for LbL films.[23-25] The main driving force for the multilayer formation is the electrostatic interaction between oppositely charged polyelectrolytes, but recently other interactions including hydrogen bonding, hydrophobic interaction, charge-transfer, and covalent bonding have been utilized.[26-28]

Here, we have investigated the influence of conformation changes of a weak polyelectrolyte, poly(acrylic acid) (PAA), on the thermoelectric performance in PANi/MWNT-PAA nanocomposites assembled *via* a LbL assembly. We have demonstrated that the thermoelectric properties, such as electrical conductivity and Seebeck coefficient, are dependent on the assembly pH conditions. Two different pH conditions, with the same components deposited in the same sequence, resulted in different thermoelectric behaviors. A 40-bilayer thin film (~210 nm thick) of PANi/MWNT-PAA assembled at pH 2.5/6.5 exhibited a power factor of 11.7 $\mu W/m \cdot K^2$, which is 50 times higher than that of the same film with all components deposited at pH 2.5. Proper control of molecular conformation resulted in a significant improvement of thermoelectric behaviour in PANi/MWNT-PAA nanocomposites through a combination of the efficient conjugate network and tightly packed nanostructure, which enhances the charge carrier mobility.

2. Experimental

2.1. Materials

Multi-walled carbon nanotubes (MWNT) (inner diameter 3-5 nm and outer diameter 10-20 nm, length 10-30 μm, purity ≥ 95%) were purchased from Cheap Tubes Inc. (Brattleboro, VT). Polyaniline (PANi) and poly(acrylic acid) (PAA) were obtained from Sigma-Aldrich (St. Louis, MO, USA). There is no further purification for all of chemicals prior to use unless otherwise stated. After manually grinding 0.1 wt% MWNTs in 0.1 wt% PAA (MW = 100,000 g/mol) using a mortar and pestle, they were bath sonicated for 20 min, followed by 30 min of 20 W tip sonication (Bandelin Sonopuls, Germany) in an ice water bath to ensure that the MWNTs were fully dispersed in solution. MWNT suspensions were then centrifuged at 4,000 rpm for 20 min, and the supernatant was decanted. 0.1 g of polyaniline (PANi, emeraldine base form, MW = 50,000 g/mol) was dissolved in 30 g of *N*,*N*-dimethyl acetamide (DMAC) (Sigma-Aldrich) by first stirring the solution overnight. Then, the PANi-DMAC solution was added to 270 mL of pH 3 water, followed by bath-sonicating for 2 h. The pH was adjusted to 2.5 with 1 M HCl and filtering through 1 μm glass filters to remove undissolved PANi particulates before the multilayer formation, in accordance with a previously reported procedure.[29]

2.2. Substrates

Poly(ethylene terephthalate) (PET) (thickness 188 μm, FilmBank, Gyeonggi-do, Korea) and single-side-polished silicon wafers (p-type, University Wafer, Boston, MA, USA) were used as the substrate for LbL assembling of the thermoelectric multilayer films. These substrates were cleaned by sequentially rinsing with DI water, methanol, and DI water and then dried with compressed air before deposition. In order to enhance the adhesion of each component by creating a negative surface charge, the cleaned PET substrates were corona-treated using a BD-20C Corona Treater (Electro-Technic Products Inc., Chicago, IL).

2.3. Layer-by-Layer assembly of PANi/MWNT-PAA thin films

PANi/MWNT-PAA multilayers were fabricated with a Multi Dip Coater robot (Hantech Co., Daejeon, Korea) on PET or Si-wafers as substrates. Each cleaned substrate was cyclically dipped into oppositely charged solutions of PANi and MWNT-PAA, respectively, along with three rinse baths of DI water between the depositions. The dipping time in the initial dips into the solutions lasted for 5 min, followed by DI water rinsing for 1 min each, which makes this cycle one bilayer (BL). After assembling the first BL, subsequent depositions were 1 min for each solution. This alternating cycle was repeated to achieve the desired number of BL. The pH of PANi was adjusted to 2.5 with either 0.1 or 1 M HCl. The pH levels of MWNT-PAA suspensions were adjusted to either 2.5 or 6.5. For the remainder of this paper PANi/MWNT-PAA nanocomposites are denoted as XPANi/Y(MWNT-PAA), where X and Y are the deposition pH of PANi and MWNT-PAA, respectively. For example, 2.5PANi/2.5(MWNT-PAA) refers to an LbL film constructed from PANi and MWNT-PAA, where the pH of both baths was adjusted to 2.5. The as-prepared PANi/MWNT-PAA films were stored in a desiccator prior to measurements. Unless otherwise stated, the outermost layer of the films used in the study was MWNT-PAA.

2.4. Characterization of thin films

The thickness of the nanocomposites was analyzed by using a NanoMap-PS contact mode stylus Profilometer. Each sample was measured five times at different locations and averaged from three different samples. Deposited mass of each layer was measured with a quartz crystal microbalance (QCM200, Stanford Research Systems, Inc., Sunnyvale, CA). Atomic force microscopy (AFM, Nanostation II™ Surface Imaging Systems, Herzogenrath, Germany) was conducted by using a non-contact mode at a scan rate of 1 Hz under ambient conditions. Surface morphology of thin films was obtained on an S-4800 Field Emission Scanning Electron Microscope (FE-SEM) (Hitachi, Japan). Free-standing films to be used for thermogravimetric analysis (TGA, PerkinElmer, TGA 8000, Ohio, USA) were deposited onto 1.6 mm polypropylene (PP) sheets purchased from AlfaAesar (WardHill, MA, USA). TGA experiments were done in nitrogen atmosphere from ambient temperature up to 1000 °C with a heating rate of 10 °C /min.

2.5. Thermoelectric characterization

A four-point probe (CMT-100S, Advanced Instrument Technology) with 0.4 mm probe tip diameter and 0.72 mm tip spacing was employed to measure the electrical resistance of the nanocomposites. The Seebeck coefficient of the films along the in-plane direction was measured with samples (25 × 10 mm) on the PET substrate under ambient conditions using a custom-built four-point probe setup (Figure S1). Two copper wires and two T-type thermocouples were used to measure electrical voltage ($\Delta V = V_{cold} - V_{hot}$) and temperature difference ($\Delta T = T_{hot} - T_{cold}$), respectively. The thermoelectric voltage induced by the temperature differentials between -10 and 10 K around room temperature was recorded by a computer equipped with LabVIEW software. The reported Seebeck coefficient was obtained using the slopes of the straight-line fits of the ΔV–ΔT curves.

3. Results and discussion

Figure 1(a) shows a schematic of the layer-by-layer (LbL) deposition process for the controlled preparation of PANi/MWNT-PAA bilayer (BL) systems, differentiated by deposition pH conditions (2.5/2.5 and 2.5/6.5). The multilayer formation is achieved by alternately immersing the substrate into positively charged PANi and anionic PAA, both of which are attached to each other through electrostatic interactions (Figure 1(b)). The MWNT nanoparticles are enveloped by the PANi and PAA during LbL assembly. An AFM image taken from a drop of the sonicated MWNT in PAA solutions on silicon wafer confirms a stable dispersion of carbon nanotubes with no precipitation over 6 months.

3.1. Film growth

A profilometer and QCM were employed to monitor the film growth of the PANi/MWNT-PAA nanocomposites, as shown in Figure 2. Both systems with two different pH conditions were linearly growing, which suggests the uniform loading of the nanotubes in each layer (Figure 2(a)). The growth rate of the multilayers at pH 2.5 is faster than that of the 2.5PANi/6.5 (MWNT-PAA) nanocomposites, achieving a thickness of 260 nm at 40 BL (2.5PANi/6.5(MWNT-PAA) was 210 nm at 10 BL). The different growth behavior can be closely related to the charge density of the weak polyelectrolyte (PAA) in the ionically bonded system. The thickness profile of the nanocomposites without

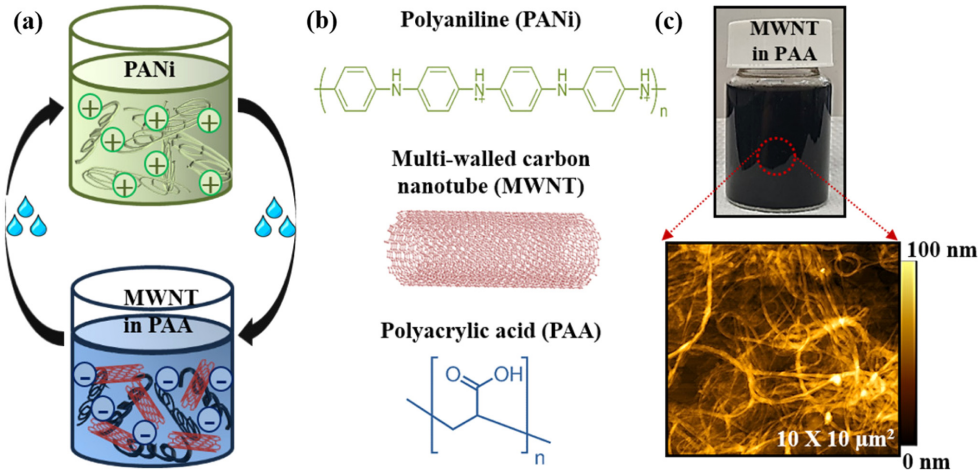

Figure 1. (a) Illustration of the layer-by-layer deposition process for the preparation of PANi/MWNT-PAA. (b) Chemical structures of polyelectrolytes and carbon nanotubes used in this study. (c) Photo image of MWNT suspensions stabilized by PAA in water and AFM image of the corresponding suspension cast onto Si-wafer.

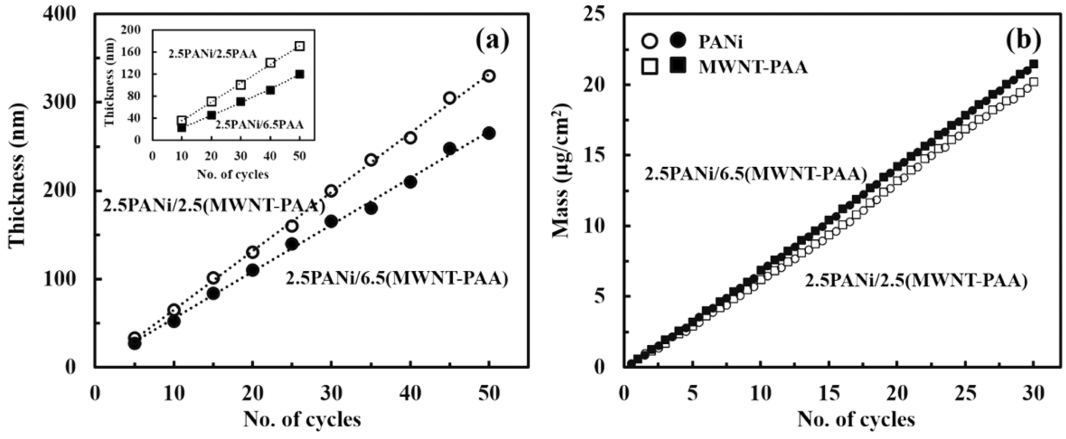

Figure 2. (a) Thickness and (b) mass growth as a function of bilayers deposited for PANi/MWNT-PAA assemblies made with two different pH conditions. The inset in the thickness profile shows growth behavior of LbL assemblies without MWNT deposited.

MWNTs deposited was evaluated to provide additional insight on the influence of assembly pH on the conformational changes of PAA. The inset in Figure 2(a) exhibited that PANi/PAA assembled at pH 2.5 was growing faster than 2.5PANi/6.5PAA. The average thickness increments of PANi and PAA layers were calculated to be 3.2 and 2.2 nm for 2.5PANi/2.5PAA and 2.5PANi/6.5PAA, respectively. Although high sensitivity of electronic properties in PANi comes from the pH conditions due to its variation on redox processes, the conformation of PANi is believed to be insensitive to pH due to rigidity of its aromatic ring structure.[30] On the other hand, a weak polyelectrolyte (PAA) is pH-responsive polymers and its conformation is variable from the charge density along the polymeric chains.[31] At low pH, PAA chains become highly protonated. With low charged state, they remain loopy and coiled due to intramolecular van der Waals attractions.[32-34] However, with increasing assembly pH, ionized COO^- groups of PAA polyelectrolytes increases.[35,36] High degree of ionization of polymeric chains induces PAA to take more extended conformation due to intrasegmental repulsion. At low pH assembly conditions, loopier and coiled PAA are deposited with each deposition step. Furthermore, the less-ionized segments of PAA are needed more to compensate the oppositely charged PANi chains, resulting in thicker films (2.5PANi/2.5PAA and 2.5PANi/2.5(MWNT-PAA)) relative to 2.5/6.5 systems.

The mass of each bilayer was measured with a QCM, as shown in Figure 2(b). Similar to the observed thickness profile, the mass increase with the number of layers deposited also displays the linear relationship. Such linear increase in mass indicates that almost the same amount of each component was loaded in each assembling step. It is interesting to observe that the mass increase as a function of layers deposited is greater for the 2.5PANi/6.5(MWNT-PAA) system. The average mass deposited for 2.5PANi/6.5(MWNT-PAA) and 2.5PANi/2.5(MWNT-PAA) films was 0.72 and 0.67 $\mu g/cm^2$, respectively. By obtaining the film thickness from profilometer and mass from QCM, the density of these two bilayers was calculated to be 1.30 and 1.01 g/cm^3 for 2.5PANi/6.5(MWNT-PAA) and 2.5PANi/2.5(MWNT-PAA) nanocomposites, respectively. The higher density of the 2.5PANi/6.5(MWNT-PAA) is likely due to a more tighly packed structure that develops during deposition. Considering the density of each component, the mass increase in the PANi/MWNT-PAA primarily comes from the nanotubes, as compared to polymers. In 2.5/6.5 system, negatively-charged PAA with flat conformation at pH 6.5 causes the films to be highly ionically-crosslinked with PANi, enveloping MWNTs to the substrate. A reduced level of ionization at pH 2.5 requires more PAA chains to compensate postively charged PANi chains. Under this circumstance, the greater amount of PAA with highly coiled/loopy conformation is expected to be deposited, accompanying less MWNTs to the films at a given assembly time. This results in reduced mass growth with lower density in the 2.5PANi/2.5(MWNT-PAA) nanocomposites relative to 2.5PANi/6.5(MWNT-PAA) films. Thermogravimetric analysis (TGA) futher confirms that a greater amount of MWNT is deposited in the 2.5PANi/6.5(MWNT-PAA) nanocomposites realtive to the 2.5PANi/2.5(MWNT-PAA) systems (Figure S2).

3.2. Thermoelectric properties

Electrical properties were studied as a function of bilayers deposited to investigate how assembly pH conditions affect performance. Sheet resistance of the nanocomposites assembled on an insulating poly(ethylene terephthalate) (PET) film was carried out by a four-point probe station, as shown in Figure 3(a). As more layers were added, the sheet resistance of both systems decreased due to increased connectivity of the MWNTs with thickness. The sheet resistance of the 2.5PANi/2.5(MWNT-PAA) films gradually decreased from 50 KΩ/sq at 10 BL to 7 KΩ/sq at 40 BL. More dramatic decrease in sheet resistance occurred in the 2.5PANi/6.5(MWNT-PAA) multilayers, exhibiting 3.5 KΩ/sq at 10 BL to 410 Ω/sq at 40 BL. Electrical conductivity was calculated by taking the inverse of the sheet resistance multiplied by film thickness (Figure 3(b)). In the 2.5PANi/2.5(MWNT-PAA) films, electrical conductivity gradually increased up to 5.4 S/cm at 40 BLs. When the assembly pH of MWNT-PAA solutions changes from 2.5 to 6.5, electrical conductivity yielded a much higher value of 95 S/cm at 40 BLs, which is almost 20 times as high as 2.5/2.5 systems. Beyond 40 BLs, the electrical properties leveled off, achieving steady state (92.8 S/cm at 50 BLs). This implies that PANi/MWNT-PAA nanocomposites have a MWNT concentration above the percolation threshold with a fully networked carbon structure.[29,37]

The Seebeck coefficient as a number of bilayers deposited is

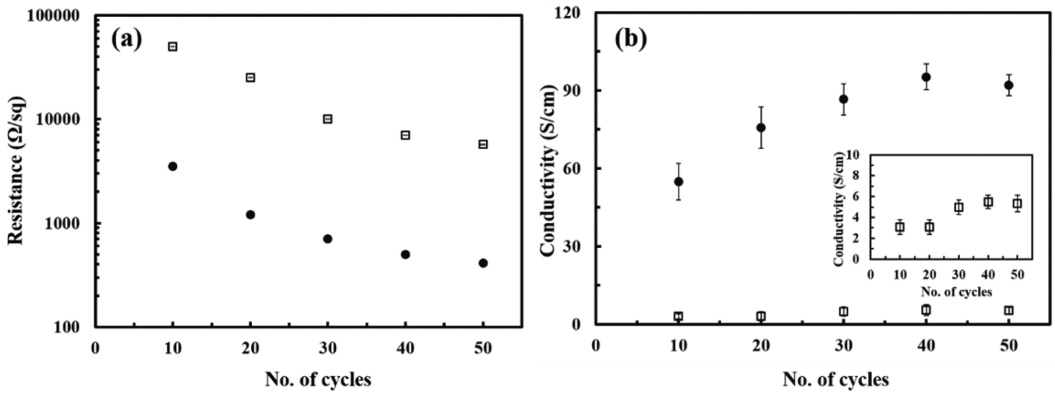

Figure 3. (a) Sheet resistance and (b) electrical conductivity as a function of bilayers deposited for PANi/MWNT-PAA nanocomposites made with two different pH conditions. The inset in the conductivity shows the electrical property of 2.5PANi/2.5(MWNT-PAA). Empty squares and filled circles are the electrical behaviors of 2.5PANi/2.5(MWNT-PAA) and 2.5PANi/6.5(MWNT-PAA), respectively.

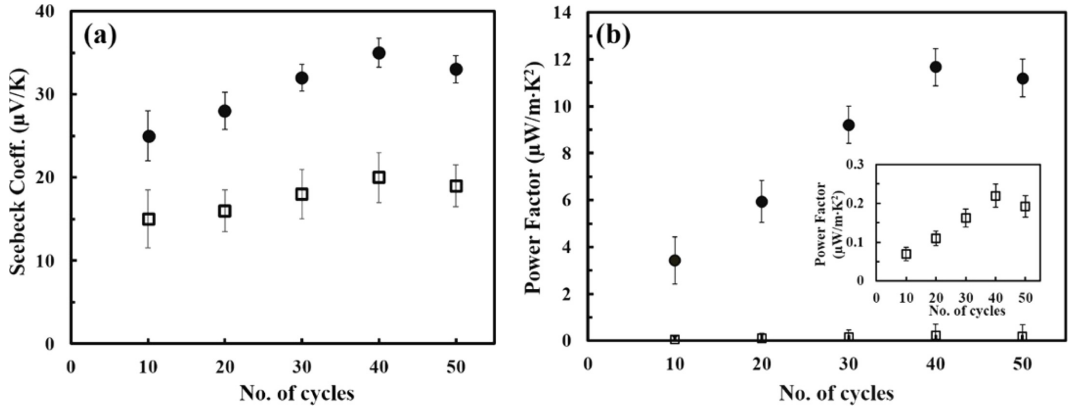

Figure 4. (a) Seebeck coefficient and (b) power factor as a function of bilayers deposited for PANi/MWNT-PAA assemblies made with two different pH conditions. The inset in the power factor shows the power factor of 2.5PANi/2.5(MWNT-PAA). Empty squares and filled circles are the thermoelectrical behaviors of 2.5PANi/2.5(MWNT-PAA) and 2.5PANi/6.5(MWNT-PAA), respectively.

shown in Figure 4(a). Both systems showed a gradual increase in Seebeck coefficient up to 40 BLs, each of which increased up to a maximum vaule of 20 and 30 μV/K for 2.5PANi/2.5(MWNT-PAA) and 2.5PANi/6.5(MWNT-PAA), respectively. The Seebeck coefficient slightly decreased after adding more layers (> 40 BLs). Similar to the trend observed with the electrical conductivity, 2.5PANi/6.5(MWNT-PAA) systems exhibited higher Seebeck coefficient relative to the nanocomposites assembled at pH 2.5, which is likely due to an efficient carrier mobility in a former structure. On the basis of the electrical conductivity and Seebeck coefficient, the power factor of the nanocomposites was calculated, as shown in Figure 4(b). With increasing number of layers, the 2.5PANi/2.5(MWNT-PAA) assemblies exbihibited an increased power factor from 0.07 at 10 BLs to 0.22 μW/m·K^2 at 40 BLs. The power factor of the 2.5PANi/6.5(MWNT-PAA) nanocomposites increased up to 11.7 μW/m·K^2 at 40 BLs, which is not only greater than that of the individual components (see Table S1), but also 50 times as large as the same film with all components deposited at pH 2.5.

Higher thermoelectric performance of 2.5PANi/6.5(MWNT-PAA) nanocomposites is attributed to more efficiently interconnected MWNTs structure. When the pH rises from 2.5 to 6.5, the polymeric chains of PAA take more extended conformation with highly charged state (Figure 5, top). Compared to coiled/loopier conformational state at low pH, such a high degree of charge density in PAA chains could induce MWNTs to be exfoliated more effectively *via* electrostatic repulsions.[38] Well-dispersed MWNTs in solutions are expected to be adsorbed parallel to the substrate while PANi and PAA are inoincally bonded, forming conjugated 3D carbon network (Figure 5, bottom) and consequenly providing efficient channels for carriers mobility. On the other hand, highly coiled conformation of PAA at low pH may not envelop enough MWNTs to create three-dimensionally aligned MWNTs-network. Instead, a larger amount of PAA chains with low charge density are randomly bonded with positively charged PANi through LbL deposition, resulting in reduction of the π-π conductive MWNT structure. A simple control on assembly pH conditions can induce conformational changes of the PAA chains, leading to different nanotube networks in the LbL films. In the present study, a high degree of charge density of PAA with flat conformation helps to achieve multidimensional

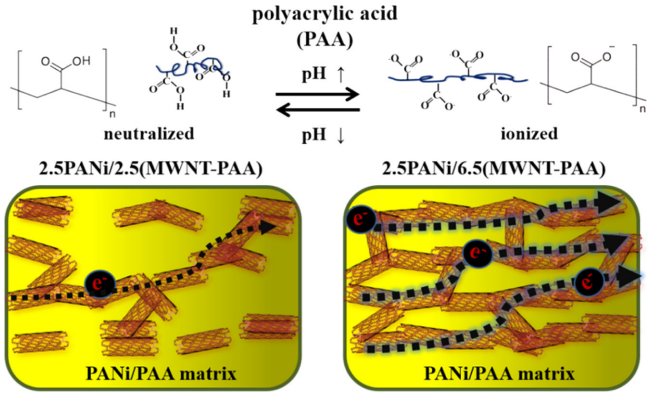

Figure 5. (Top) Molecular structures of PAA depending on pH conditions and (bottom) schematic of the MWNTs network in the PANi/MWNT-PAA nanocomposites created with two different pH conditions.

conjugated nanostructures, enhancing electrical conductivity and carrier mobility (hence, thermoelectric performance).

3.3. Surface structure

In an effort to observe the surface morphology of the 2.5PANi/6.5(MWNT-PAA) nanocomposites, we carried out AFM and SEM analysis, as shown in Figure 6. PANi/PAA films without MWNT deposited displayed the film surface with relatively smooth and a featureless surface morphology (Figure 6(a,c)). Highly stabilized MWNTs in the aqueous solution of PAA were uniformly deposited onto the multilayers, as could be seen from Figure 6(b). The inset in the SEM image further confirmed completely exfoliated single nanotubes and their bundles interwoven with one another on the surface of the 2.5PANi/6.5(MWNT-PAA) nanocomposites. The AFM height image of a 3 BL film clearly showed taht the films have an interconnected network structure with uniformly dispersed MWNTs (Figure 6(d)). A highly conjugated network with excellent MWNT coverage was achieved with only a few deposition cycles. A three-dimensional achitecture with highly entangled nanotube structures created *via* an LbL assembly translates into the formation of an extensive network of conductive pathways. This feature provides an efficient pathway for carriers

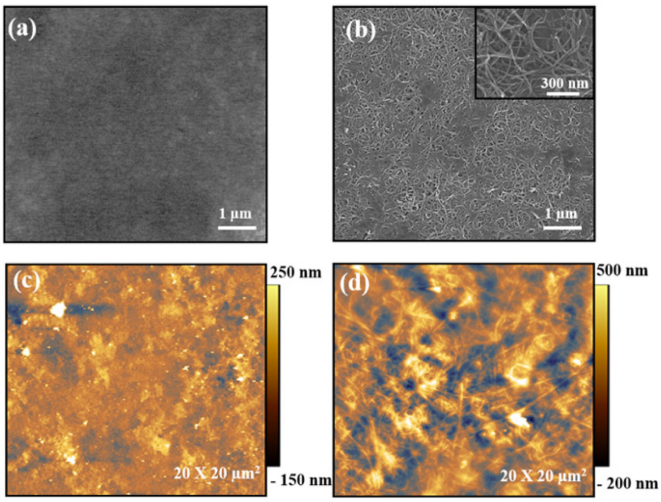

Figure 6. SEM images of (a) 2.5PANi/6.5PAA and (b) 2.5PANi/6.5 (MWNT-PAA) nanocomposites. AFM height images of (c) 2.5PANi/6.5PAA and (d) 2.5PANi/6.5(MWNT-PAA) nanocomposites. The inset in the SEM image shows higher resolution MWNT.

transport under temperature differentials, consequently boosting up the thermoelectric properties.

4. Conclusions

In summary, we have demonstrated that assembly pH conditions altered the film's growth, structure, and properties. The influence of pH conditions on molecular conformation in governing the thermoelectric properties of the organic materials was highlighted. The 2.5PANi/6.5(MWNT-PAA) multilayer had a more dense structure due to high charge density of a weak polyelectrolyte (PAA) relative to the counterpart assembled at 2.5/2.5. The densely packed 2.5PANi/6.5(MWNT-PAA) multilayer (40 BL was ~ 210 nm thick) demonstrated high thermoelectric performance due to an efficient conjugated π-π network, achieving an electrical conductivity of 95.2 S/cm and a Seebeck coefficient of 35 μV/K. This translates to a power factor of 11.7 $\mu W/m{\cdot}K^2$, which is 50 times higher than that of the same film with all components deposited at pH 2.5. The results revealed in this study not only demonstrate a simple control of solution pH during layer-by-layer assembly is the key to enhance thermoelectric performance but also indicate pH-sensitive polyelectrolytes are good candidates to deepen the understanding of the critical structure-morphology-function relationship in thermoelectric materials.

Supporting information: Information is available regarding the schematic of a home-built four-point probe apparatus, thermoelectric properties of polyaniline and MWNT, and TGA thermograms of PANi/MWNT-PAA systems. The materials are available *via* the Internet at http://www.springer.com/13233.

References

(1) N. Bizon, N. M. Tabatabaei, F. Blaabjerg, and E. Kurt, *Energy Harvesting and Energy Efficiency*, Springer, 2017.
(2) H. Teng, B. Kok, C. Uttraphan, and M. Yee, *Int. J. Renew. Energy Res.*, **8**, (2018).
(3) H. Shi, Z. Liu, and X. Mei, *Energies*, **13**, 86 (2020).
(4) J. Chen and Z. L. Wang, *Joule*, **1**, 480 (2017).
(5) G. Liu, J. Chen, H. Guo, M. Lai, X. Pu, X. Wang, and C. Hu, *Nano Res.*, **11**, 633 (2018).
(6) E. A. Scott, J. T. Gaskins, S. W. King, and P. E. Hopkins, *APL Mater.*, **6**, 058302 (2018).
(7) B. Russ, A. Glaudell, J. J. Urban, M. L. Chabinyc, and R. A. Segalman, *Nat. Rev. Mater.*, **1**, 16050 (2016).
(8) D. Teweldebrhan, V. Goyal, and A. A. Balandin, *Nano Lett.*, **10**, 1209 (2010).
(9) X. Shi, L. Chen, and C. Uher, *Int. Mater. Rev.*, **61**, 379 (2016).
(10) Y. Wang, Y. Sui, H. Fan, X. Wang, Y. Su, W. Su, and X. Liu, *Chem. Mater.*, **21**, 4653 (2009).
(11) S. Peng, D. Wang, J. Lu, M. He, C. Xu, Y. Li, and S. Zhu, *J. Polym. Environ.*, **25**, 1208 (2017).
(12) M. Culebras, K. Choi, and C. Cho, *Micromachines*, **9**, 638 (2018).
(13) J. L. Blackburn, A. J. Ferguson, C. Cho, and J. C. Grunlan, *Adv. Mater.*, **30**, 1704386 (2018).
(14) J. P. Jurado, B. Dörling, O. Zapata-Arteaga, A. Roig, A. Mihi, and M. Campoy-Quiles, *Adv. Energy Mater.*, **9**, 1902385 (2019).
(15) K. Xu, G. Chen, and D. Qiu, *Chem. Asian J.*, **10**, 1225 (2015).
(16) W. Wang, S. Sun, S. Gu, H. Shen, Q. Zhang, J. Zhu, L. Wang, and W. Jiang, *RSC Adv.*, **4**, 26810 (2014).
(17) G. P. Moriarty, J. N. Wheeler, C. Yu, and J. C. Grunlan, *Carbon*, **50**, 885 (2012).
(18) C. Cho, K. L. Wallace, P. Tzeng, J. H. Hsu, C. Yu, and J. C. Grunlan, *Adv. Energy Mater.*, **6**, 1502168 (2016).
(19) H. J. Lee, G. Anoop, H. J. Lee, C. Kim, J.-W. Park, J. Choi, H. Kim, Y.-J. Kim, E. Lee, and S.-G. Lee, *Energy Environ. Sci.*, **9**, 2806 (2016).
(20) C. Cho, M. Culebras, K. L. Wallace, Y. Song, K. Holder, J.-H. Hsu, C. Yu, and J. C. Grunlan, *Nano Energy*, **28**, 426 (2016).
(21) X. Zhang, Y. Xu, X. Zhang, H. Wu, J. Shen, R. Chen, Y. Xiong, J. Li, and S. Guo, *Prog. Polym. Sci.*, **89**, 76 (2019).
(22) K. Ariga, E. Ahn, M. Park, and B. S. Kim, *Chem. Asian J.*, **14**, 2553 (2019).
(23) A. Palanisamy, V. Albright, and S. A. Sukhishvili, *Chem. Mater.*, **29**, 9084 (2017).
(24) E. A. Nagelli, L. Huang, A. Q. Z. Dai, F. Du, and L. Dai, *Part. Part. Syst. Charact.*, **34**, 1700131 (2017).
(25) R. McNeil Jr. and P. J. Paukstelis, *Adv. Mater.*, **29**, 1701019 (2017).
(26) R. Gao, X. Fang, and D. Yan, *J. Mater. Chem. C*, **6**, 4444 (2018).
(27) G. Liu, Z. Jiang, C. Chen, L. Hou, B. Gao, H. Yang, H. Wu, F. Pan, P. Zhang, and X. Cao, *J. Membr. Sci.*, **537**, 229 (2017).
(28) Q. An, T. Huang, and F. Shi, *Chem. Soc. Rev.*, **47**, 5061 (2018).
(29) C. Cho, S. Qin, K. Choi, and J. C. Grunlan, *ACS Appl. Polym. Mater.*, **1**, 1942 (2019).
(30) T. Lindfors and A. Ivaska, *J. Electroanal. Chem.*, **531**, 43 (2002).
(31) C. Wang and K. Tam, *J. Phys. Chem. B*, **108**, 8976 (2004).
(32) Y. Roiter and S. Minko, *J. Phys. Chem. B*, **111**, 8597 (2007).
(33) Y.-H. Yang, M. Haile, Y. T. Park, F. A. Malek, and J. C. Grunlan, *Macromolecules*, **44**, 1450 (2011).
(34) S. S. Shiratori and M. F. Rubner, *Macromolecules*, **33**, 4213 (2000).
(35) C. Cho, L. Valverde, G. A. Ozin, and N. S. Zacharia, *Langmuir*, **26**, 13637 (2010).
(36) C. Cho and N. S. Zacharia, *Langmuir*, **28**, 841 (2012).
(37) C. Cho and J. Son, *Nanomaterials*, **10**, 41 (2020).
(38) M. Olek, J. Ostrander, S. Jurga, H. Möhwald, N. Kotov, K. Kempa, and M. Giersig, *Nano Lett.*, **4**, 1889 (2004).